Dust devil speeds, directions of motion and general characteristics observed by the Mars Express High Resolution Stereo Camera

Christina Stanzel, Martin Pätzold, David A. Williams, Patrick L. Whelley, Ronald Greeley, Gerhard Neukum

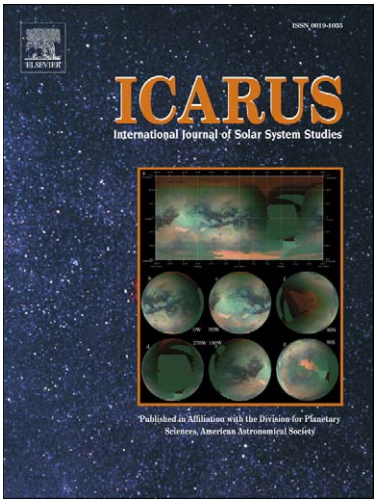

Dust devil speeds, directions of motion and general characteristics observed by the Mars Express High Resolution Stereo Camera

Christina Stanzel, Martin Pätzold, David A. Williams, Patrick L. Whelley, Ronald Greeley, Gerhard Neukum

PII: S0019-1035(08)00187-5
DOI: 10.1016/j.icarus.2008.04.017
Reference: YICAR 8675

To appear in: *Icarus*

Received date: 14 June 2007
Revised date: 20 March 2008
Accepted date: 30 April 2008

Please cite this article as: C. Stanzel, M. Pätzold, D.A. Williams, P.L. Whelley, R. Greeley, G. Neukum, Dust devil speeds, directions of motion and general characteristics observed by the Mars Express High Resolution Stereo Camera, *Icarus* (2008), doi: 10.1016/j.icarus.2008.04.017

Dust devil speeds, directions of motion and general characteristics observed by the Mars Express High Resolution Stereo Camera

Christina Stanzel,[a,*] Martin Pätzold,[a] David A. Williams,[b] Patrick L. Whelley,[b,c] Ronald Greeley,[b] Gerhard Neukum[d] and the HRSC Co-Investigator Team

[a] Department of Planetary Research, Rhenish Institute of Environmental Research at the University of Cologne, Aachener Strasse 201-209, 50931 Cologne, Germany

[*] Corresponding Author E-mail address: christina.stanzel@uni-koeln.de

[b] School of Earth and Space Exploration, Arizona State University, Box 871404, Tempe 85287-1404, Arizona, USA

[c] Now at: Department of Geology, University at Buffalo, SUNY, 875 Natural Sciences Complex, Buffalo, New York, USA 14260-3050

[d] Institute of Geological Sciences, Freie Universität Berlin, Malteserstr. 74-100, 12249 Berlin, Germany

Pages: 46

Tables: 3

Figures: 7

Proposed Running Head: HRSC Dust Devils

Editorial correspondence to:

Christina Stanzel

Abteilung Planetenforschung

Rheinisches Institut für Umweltforschung an der Universität zu Köln

Aachener Strasse 209

50931 Köln

Germany

Phone: +49-221-27781812

Fax: +49-221-400-2320

E-mail address: christina.stanzel@uni-koeln.de

ABSTRACT

A total of 205 dust devils were detected in 23 High Resolution Stereo Camera (HRSC) images taken between January 2004 and July 2006 with the ESA Mars Express orbiter, in which average dust devil heights were ∼660 m and average diameters were ∼230 m. For the first time, dust devil velocities were directly measured from orbit, and range from 1 to 59 m/s. The observed dust devil directions of motion are consistent with data derived from a General Circulation Model (GCM). In some respects HRSC dust devil properties agree favorably with data from the NASA Mars Exploration Rover Spirit dust devil analyses. The spatial distribution of the active dust devils detected by HRSC supports the conjecture that the ascending branch of the Hadley circulation is responsible for the increase in dust devil activity, especially observed during southern summer between 50° and 60°S latitude. Combining the dust-lifting rate of 19 kg/km^2/sol derived from the Spirit observations with the fewer in number but larger in size dust devils from various other locations observed by HRSC, we suggest that dust devils make a significant contribution to the dust entrainment into the atmosphere and to the Martian dust cycle.

Key Words: Mars; Mars Atmosphere; Mars Surface; Atmospheres Dynamics; Meteorology

1. Introduction

Dust devils are thermally driven atmospheric vortices that are filled with loose material such as sand and dust (Sinclair, 1969). The particles are raised from the surface by the low-pressure core within the dust devil, which was found to be a very effective way to move even fine-grained particles (Greeley et al., 2003; Ferri et al., 2003; Balme and Hagermann, 2006). Dust devils are visible by their dust-filled columns. They are seen as bright features illuminated by the Sun and emphasized by an elongated dark shadow. The existence of such atmospheric vortices was predicted for Mars (Ryan, 1964; Neubauer, 1966; Gierasch and Goody, 1973) before they were first detected in Viking images (Thomas and Gierasch, 1985). Both Viking orbiters imaged dust devils, and data recorded by the two Viking landers suggested the passage of several vortices that were likely dust devils (Ryan and Lucich, 1983; Ringrose et al, 2003). Cantor et al. (2006) conducted a survey over almost four Mars years using Mars Orbiter Camera (MOC) images on board the NASA Mars Global Surveyor (MGS). They showed that dust devils are a common feature and widespread over Mars, occurring at almost all elevations. Dust devils on Mars and Earth are most likely to form in spring and summer (Cantor et al., 2006; Balme et al., 2003) at noon and just afternoon (Sinclair, 1969; Wennmacher et al., 1996; Balme et al., 2003). Their size ranges from a few to hundreds of meters in diameter, with heights between a few meters and to several kilometers (Thomas and Gierasch, 1985; Edgett and Malin, 2000; Biener et al., 2002).

The variety in sizes, the numerous occurrences, and the effective dust-lifting ability suggests that dust devils play an important role in the thermal structure of the atmospheric boundary layer of Mars (Zurek et al., 1992). They contribute to Martian weather by dust entrainment, which influences atmosphere temperature, and lead to surface changes by removing thin layers of dust, causing albedo changes (Malin and Edgett, 2001). Studies on Earth (Ives, 1947; Ryan, 1972; Snow and McClelland, 1990; Metzger, 2003) and Mars (Cantor et al., 2006; Balme et

al., 2003; Fisher et al., 2005) have been conducted to better understand their dynamics and impact on the atmosphere and climate, especially for Mars. Most investigations concentrated on specific study areas, extrapolating the spatial and temporal distribution of dust devils to larger regions. Consequently, the full extent of the contribution to the dust budget is poorly known. Additionally, models have been developed and compared (Kanak, 2006) to understand when, where, and under which circumstances dust devil-like vortices form. Laboratory work (Neakrase et al., 2006; Greeley et al., 2004; Greeley et al., 2003) has been conducted to simulate dust flux within dust devils, the directions of motion, and particle lifting under Martian conditions to understand the basic dynamics and characteristics of dust devils. The nearly global coverage of Mars by HRSC and the in situ images by the rovers shed light on many aspects of dust devils. This paper extends our initial report of dust devils detected with HRSC on the ESA Mars Express orbiter (Stanzel et al., 2006) by including new HRSC data and the Super Resolution Channel (SRC) with observations of active dust devils. We relate our findings from HRSC/SRC to the recent analyses of dust devils using the Mars Exploration Rover Spirit (Greeley et al., 2006) and Pathfinder data (Metzger et al., 1999; Ferri et al., 2003), which provide new insight into the dynamics of dust devils on Mars, when compared with recent dust devil studies (Neakrase et al., 2006; Balme and Hagermann, 2006; Whelley and Greeley, 2006; Cantor et al., 2006).

2. HRSC observations

2.1 Spatial and temporal distribution and dimensions

A total of 205 dust devils have been observed as of July 2007 in HRSC images from 23 different Mars Express orbits; of these, the forward motion for 194 could be tracked. The observations range from January 2004 to July 2006, covering northern and southern hemispheres at various seasons. Constraints on this study include at first no systematic search for dust devils, and

there was no favoring of certain times of day or seasons for dust devil examination. Several regions of Mars were subjected to focused study, including Amazonis Planitia (where many dust devils have been found previously: Cantor et al., 2002; Fisher et al, 2005; Cantor et al., 2006), Chryse Planitia and Syria Planum. Chryse Planitia was chosen, because it is a northern lowland including the Viking 1 and Pathfinder landing sites, which are known as active dust devil areas, and Syria Planum, because it is a known region for dust devils and dust storms. The parameters of each orbit where dust devils have been detected, as well as the dust devil characteristics (speeds, diameters and heights), are listed in Table 1, and the spatial coverage is presented in Figure 1.

[**Table 1**]

[**Figure 1**]

The majority of the dust devils in the southern hemisphere (70 of 95 or 73.7%) were found between 50° and 60°S latitude at local summer. The dust devils were not detected in any single region, but occur at longitudes from 14°E to 170°E. These dust devils are typical, with diameters of ∼100 to ∼500 m and heights of ∼200 to ∼1000 m (only two dust devils were >1500 m). Further detections in the southern hemisphere include Syria Planum, Thaumasia Planum, Icaria Planum, Syrtis Planum and near Vallis Marineris. In Amazonis and Arcadia Planitia and in the southern parts of Chryse Planitia/Simud Vallis, dust devil detections were made in the northern hemisphere, with 99 of 110 of these dust devils (90%) in Chryse Planitia/Simud Vallis alone. Overall, 53.7% of the dust devils were seen in the northern hemisphere, and 46.3% in the south. Malin and Edgett (2001) reported streaks interpreted as dust devil tracks at nearly all latitudes and elevations. We observed active dust devils in northern desert plains several kilometers below the reference aeroid, as well as in southern plateaus and cratered highlands, including the floor of Peneus Patera (Oberst et al., 2008). Dust devil tracks have also been seen in the caldera of Arsia Mons in both MGS MOC and HRSC images.

The frequency of occurrence is quite different for the three target areas Amazonis Planitia, Chryse Planitia and Syria Planum. The respective images were selected by searching for all HRSC images that cover the predefined latitude and longitude range of the target area, even for small areas. For this reason, adjacent regions and probable dust devil detections may be added to the target areas. Amazonis Planitia shows the lowest frequency of dust devils, with only 2.3% (2) of the analyzed 87 images including dust devils. This results in 0.1 dust devils per image. Syria Planum shows a frequency of 0.5 dust devils per image, where 17.6% (8) of the 17 images show dust devil activity. Chryse Planitia had the highest quantity with 30.8% (8) of the 17 images containing dust devils, which results in 4.2 dust devils per image. Summing up the results of the target regions, we found dust devils in 10% of the analyzed images. If dust devils occurred, it averages to 9.5 dust devils per image.

Dust devils were found in all seasons on both hemispheres (Figure 2).

[**Figure 2**]

The majority of dust devils in the northern hemisphere were detected in Martian spring, but were also frequent in fall and winter seasons. Surprisingly, the fewest dust devils were detected in the summer. This observation can be partly related to a latitudinal bias, in which most dust devil detections in the northern hemisphere were close to the equator, where the season does not dominantly control dust devil activity. The dust devil distribution in the southern hemisphere has a clear peak during southern summer, consistent with Whelley and Greeley (2006 and in press), with very few detections in the other seasons (Figure 2). All dust devils detected by HRSC occurred at noon or afternoon (Figure 3), as on Earth (Sinclair, 1969; Snow and McClelland, 1990) and in previous Mars studies (Wennmacher et al., 1996; Balme et al., 2003; Greeley et al., 2006). The data shows a significant peak between 1400 and 1500 hours.

[**Figure 3**]

The diameters of most observed dust devils were between 100-400 m. Exceptions were two

objects that lacked well defined vortices, which are most likely large dust clouds ∼650 and ∼1430 m across. The largest dust devil seen in HRSC images was ∼1650 m in diameter and ∼4440 m high, while the smallest was 80 m in diameter and ∼110 m high. The average size was ∼230 m in diameter and ∼660 m high, consistent with the findings on narrow angle (NA) MOC images by Fisher et al. (2005).

2.2 Traverse velocities and directions of motion

The unique imaging capability of the HRSC enables the forward velocities of dust devils to be computed from their positions in three stereo channels (nadir (ND), stereo-1 (S1), and stereo-2 (S2)) and the time they were imaged. Dust devils could not always be recognized in all three HRSC images, either because they disappeared in the time between acquisitions of two HRSC channels, or because the image resolution of an individual channel was too low. Typically, the Martian surface is imaged with the ND channel at the best resolution (12.5 m/pixel) and with the S1 and S2 channels at 25 m/pixel. All calculations of dust devil diameter and height, discussed above, were done using the highest resolution data, typically the ND channel. The derived speeds of dust devils seen in one orbit are consistent and most dust devils despite their separations moved in the same direction. The traverse velocities can therefore be considered as ambient wind speeds and near-surface values, as discussed by Stanzel et al. (2006). The larger parts of the detected dust devils have a forward motion range from a few meters per second to 15 m/s (Table 1). These values are in good agreement with observations of dust devils on Earth (Sinclair, 1969; Snow and McClelland, 1990) and with predictions for Mars (Ryan and Lucich, 1983; Metzger et al., 1999; Rennó et al., 1998; Ferri et al., 2003). The average speed for 74 dust devils, however, was 23.1 m/s, with a range from 15.0 to ∼59 m/s (Table 1).

As a consequence of Martian high wind speeds the core diameters of dust devils are thought to be larger according to theory (increase in ambient vorticity; Rennó et al., 2000). No such

correlation is apparent in the HRSC data, however. Only the dust devils in Amazonis Planitia have diameters <100 m and low speeds. There are, however, dust devils in Syria Planum (orbit 2032) with small diameters of 80 and 138 m and average speeds of 20 m/s. The largest diameters (orbit 2054) have been seen at high speeds. However, the images of the three stereo channels are 'snap-shots' and do not indicate longer duration observations. The smaller dust devils formed at high speeds might have just formed and were still growing (Rennó et al., 2000). The direction of motion was derived for each dust devil where possible but maps are only prepared for the southern Chryse Planitia/Simud Vallis/Vallis Marineris region and the 50°-60°S latitude range for selected longitudes, because here are more than 20 dust devils available for statistical purposes. Figure 4 shows the maps for the Chryse Planitia/Simud Vallis/Vallis Marineris and the Peneus Patera region.

[**Figure 4**]

Figure 4a shows dust devil directions of motion from 8 orbits covering spring, fall and winter times (relating to northern hemisphere). Remarkable are the almost opposite directions of motion in spring and winter times. This can be clearly seen although the data do not spatially overlap very much. The directions of motion seen in fall correspond quite well to the winter data.

These data can now be used either to verify model output showing the directions of motion of the general circulation, or to identify a local spatial or temporal anomaly of the general circulation. Values of the wind speed components in east- and northward directions have been used from the Martian Climate Database (http://www-mars.lmd.jussieu.fr/) to derive the wind direction in an altitude of 10 m above the surface. The simulation for the spring shows northward and north-north-eastward directions for the 10°-20° latitude range in the southern parts of Chryse Planitia. The dust devils were moving mostly in northward to northwestward directions, although three dust devils moved to the south. The more western directions of

motion of the dust devils are probably due to the flow field existing in the broad valley system. The southern directions of motion of dust devils in winter times correspond favorably to the appropriate Hadley circulation, where the near-surface flow comes from northern latitudes, and crosses the equator up to southern mid-latitudes. In the range of 10°S latitude (Vallis Marineris) the dust devils show no preferential direction of motion, probably due to the more chaotic winds in the valley system. Figure 4b (Peneus Patera) shows two orbits with 21 directions of motion of dust devils at southern summer times. According to the Hadley circulation all dust devils are moving to south-eastern directions and show as well the Coriolis acceleration to the left on the southern hemisphere. The data from the Martian Climate Database show no deviation from these measurements.

In the Terra Cimmeria region (orbit 2242, not shown) 19 directions of motion could be derived from 26 dust devils. Here, in contrast to the other dust devils in the 50°-60°S latitude range, no preferential direction of motion could be seen, but between 60°-62°S latitude with an eastward flow (corresponding to the results in Peneus Patera, Figure 4b). The directions of motion of five dust devils at ∼52°S and ∼56°S latitude, respectively, show completely different and sometimes opposite directions.

2.3 Active dust devil seen in SRC image

One dust devil was observed on the caldera floor of Peneus Patera by both the HRSC and the SRC (Figure 5; see also Oberst et al., 2008).

[**Figure 5**]

This is very fortunate because SRC images are not obtained on every orbit and they typically cover only a small strip imbedded in the centre of the nadir images. The dust devil and its shadow are clearly visible, although it is at the image border of the SRC image. Nevertheless, this example shows the potential of the SRC. While the resolution of the ND channel was only

25 m/pixel (Figure 5a), the SRC image at 5 m/pixel reveals more details of the structure of the dust devil, as well as of the surrounding environment (Figure 5b). In addition, streaks inferred to be dust devil tracks can be identified and placed in the broader context of the HRSC image, suggesting that the floor of Peneus Patera is covered with dust. The dust devil is tilted in the direction of the shadow in the ND image. The analysis of the SRC image shows a clear kink between the lower, thinner, columnar vortex, and the upper broad, expanded vortex (likely due to wind shear) of the dust devil (Figure 5c). The 'kink' is in the direction of the shadow and cannot be seen in the shadow itself, so the altitude of the wind shear cannot be retrieved.

The direction of tilt of dust devils is assumed to indicate their direction of motion (Rennó et al., 2000; Greeley et al., 2006). The sequential position of the dust devil is in the direction of the kink, in agreement with the first position seen. We conclude that the wind shear tilts the dust devil in the wind direction and that the ambient wind moves it forward.

The better resolution of SRC images also enabled a better measure of the dust devil diameter. For example, the lower columnar vortex appeared to be 90 m in the HRSC ND channel, but 42 m in the SRC image. This suggests that the diameters obtained for the HRSC ND are overestimates. We found no significant difference in the shadow length and therefore the height (1352 vs. 1366 m), between the HRSC ND and SRC data.

2.4 Lifetime

Dust devils are occasionally observed creating new tracks seen from Spirit (Greeley et al., 2006), and from orbit in MOC images (Cantor et al., 2006). Seven active dust devils were observed with HRSC in orbit 2225 leaving tracks in southern Noachis Terra (Figure 6). They are surrounded by an abundance of other streaks.

[Figure 6]

Assuming that dust devils create tracks once they start moving and that they collapsed where

the streaks terminate, we computed the potential lifetime of dust devils by using the measured speeds of active dust devils and the lengths of their tracks. Tracks created by observed dust devils were used along with tracks in the vicinity of dust devils 3-6 (Figure 6) in orbit 2225 (Table 1). The assumed speed for the tracks is 6 m/s, which is the average for the four active dust devils. The shortest lifetime was less than four minutes for a dust devil which moved ∼1850 m at 8.4 m/s. The longest lifetime was about 32 minutes for a distance of 11.7 km at 6 m/s. The mean value for 12 analysed tracks is about 13 minutes.

3. Comparison and discussion

3.1 HRSC versus Lander observations

Lander and orbiter investigations differ mostly from the imaging method. Pathfinder and Spirit took images including the horizon to better resolve dust devils due to the contrast between the surface and the sky. Contrast enhancements (Ferri et al., 2003; Greeley et al., 2006) or wavelength comparisons (Metzger et al., 1999) were necessary to resolve dust devils in images from the surface. These images are broader in the horizontal direction relative to the vertical direction, such that the tops of dust devils are often cut off, but as many dust devils as possible are included. This limits the estimation of the heights of dust devils. Additionally, the distance, speed and direction of motion are more difficult to determine than from orbiter images. The field of view and the height above the ground of the camera are further limitations. Spirit could choose one viewing direction per sol (Greeley et al., 2006), but local topographic variations may hide dust devils. Rover dust devil observations may also be restricted due to power constraints, and the observing distance of rovers or landers compared to orbiters is limited.

Nevertheless, dust devil detections in orbiter images are mostly by chance, while for example Spirit conducted special dust devil campaigns. Observations were done in the middle of the day when dust devils are most likely to be present. This led to the higher number of dust devil

observations in lander images.

3.1.1 Dimensions

[**Table 2**]

Our research has found that lander and orbiter observations complement each other (Table 2). The smallest dust devils observed in HRSC images have diameters of 50 m, which are four image pixels at the highest resolution of 12.5 m/pixel in the HRSC ND channel. Most dust devils seen by Spirit were 10 to 20 m in diameter, or roughly one third of the smallest dust devil diameters observed by HRSC. The largest diameter from Spirit observations was 276 m, which is in the range of most of the HRSC-observed dust devils (<400 m in diameter). These results are also consistent with Pathfinder data (Metzger et al., 1999; Ferri et al., 2003).

We suggest that conclusions about dust devil frequency made by several authors who examined images from different orbiter missions must now be reassessed, because the smaller dust devils observed by landers are typically not seen from orbit. This is exemplified by the difference in the total number of dust devils observed by HRSC and Spirit. Spirit has seen many more, but much smaller dust devils.

3.1.2 Time of day

The time of occurrence using all HRSC-observed dust devils is in good agreement with Spirit/-Pathfinder-observed dust devils. A diurnal distribution of dust devil occurrence cannot be retrieved from MOC data, because the observations are limited to 1300-1500 hours local time. The distribution of dust devils seen in HRSC (Figure 3) and Spirit/Pathfinder data compare favorably with terrestrial observations, in which dust devil activity starts in the morning around 1000-1100 hours, peaks at 1300-1400 hours, and tends to vanish after 1600-1700 hours (Sinclair, 1969). The HRSC-observed dust devil peak is between 1400-1500 hours, but shows a

higher frequency during the whole afternoon between 1200 to 1600 hours, with a break between 1300-1400 hours. Confirmed convective vortices measured by the Mars Pathfinder Atmospheric Structure Investigation/Meteorology (ASI/MET) experiment occurred between 0930-1700 local time (Murphy and Nelli, 2002), which agrees favorably with our data.

3.1.3 Speed

The translational speeds of dust devils are a few meters per second as reported in most cases (Ryan and Lucich, 1983; Metzger et al., 1999; Rennó et al., 1998; Ferri et al., 2003), if ambient winds are low or it is calm. However, dust devils exist at and move with high wind speeds as well, including the best-developed and largest dust devils observed with HRSC (Figure 7).

[**Figure 7**]

One explanation for the relatively high speeds of the five dust devils detected in Thaumasia Planum (Figure 7a), which moved all in one row, is that they may have developed at an air mass boundary (Stanzel et al., 2006). We infer that they moved across the surface at high wind speeds which are commonly found along such fronts.

The two orbits covering Syria Planum (2032 and 2054) showed seven dust devils and revealed another explanation for their relatively high speeds. The images, taken only 7.4 Mars days apart from each other, include a small and a large dust storm. Cantor et al. (2006) showed several MOC images where large dust devils and plumes occurred at the fronts of dust storms. They relate them to terrestrial vortices accompanying passing storm fronts. So the dust storms seen by HRSC may be responsible for the fast motion and the initiation of the dust devils. The dust devils seen at the front of the storm (Figure 7b) indicate with their computed speeds as well the speed of the dust storm if they are propelled by the storm. This is supported by the simulations by Toigo et al. (2003), in which dust devils developed both in the 'highest wind speed' case and in the 'no background wind' case.

Former investigations concerning dust devils on Earth and Mars assume that high ambient wind speeds suppress dust devil formation and evolution and that measurements of high forward motions are due to measurement errors (Snow and McClelland, 1990). Combining existing theory and simulations (Kanak, 2006; Michaels and Rafkin, 2004; Rennó et al., 2000; Rennó and Bluestein, 2001) with the results from HRSC and Spirit (<1-21 m/s) leads to the suggestion that dust devil formation is not suppressed by high wind speeds.

3.1.4 Lifetime

Twelve dust devils observed in HRSC images were used to calculate their lifetimes for comparison with those derived from Gusev dust devils (Table 2). The lifetimes agree very well with each other. Sinclair (1969) noted that most terrestrial dust devils last only for a few minutes, with some as long as 20 minutes, although some exceptions of several hours duration are mentioned. Long durations occur when dust devils are stationary, and if there is sufficient warm air and a supply of particles (Ives, 1947). In addition the duration depends on the size of dust devils with larger dust devils lasting longer and traveling further. These relations appear to be true on Mars as well. The computed lifetimes for Martian dust devils may be a lower limit because the visible dust devil is used as the end point, and the vortex is likely to continue to exist even without entrained dust. The tracks are used as a measure for the travel distance (including the starting point), but as stated above and as seen in most of the orbits here, dust devils may occur without leaving visible tracks. Understanding the duration of Martian dust devils is important to obtain a better estimation of the dust entrainment into the atmosphere based on frequency, size, and flux of dust in dust devils.

3.1.5 Dust-lifting Rate

The magnitude of the dust flux and the mechanism of dust entrainment into the atmosphere

remain uncertain. Smaller, tighter vortices are more efficient in lifting dust (Neakrase et al., 2006). The dust flux increases with larger pressure wells. This is confirmed by the theoretical work of Balme and Hagermann (2006). The quantitative analysis by Greeley et al. (2006) using Spirit data demonstrates the large amount of dust that is lifted by many small size dust devils. These simulations, theories, and image analyses prove the contribution of dust devils to the dust cycle of Mars. Larger dust devils as seen by HRSC can carry dust several kilometers high where it may remain in suspension. Depending on their potentially longer lifetime and larger size, the HRSC-observed dust devils provide an additional contribution to the amount of lifted dust of 19 kg/km^2/sol calculated by Greeley et al. (2006).

We computed the amount of dust lifted by typical HRSC-observed dust devils (diameter 230 m, duration 790 s, travel distance 4300 m) by determining the areal extent of the dust devils interaction with the surface and multiplying that by published dust devil flux and frequency measurements (Table 3).

[**Table 3**]

The area from which dust is lifted is calculated first as the dust devil area with πr^2 ($4.2{*}10^4$ m^2), and secondly as the area of the travel distance, diameter$*$distance ($9.9{*}10^5$ m^2). Different dust fluxes used were derived from observations by Spirit (Greeley et al. (2006): $2{*}10^{-5}$ kg/m^2/s), Mars Pathfinder (Metzger et al. (1999): $5{*}10^{-4}$ kg/m^2/s) and MOC (Cantor et al. (2006): $1{*}10^{-9}$ kg/m^2/s), and from laboratory work (Neakrase et al. (2006): $1{*}10^{-3}$ kg/m^2/s). The results of Whelley and Greeley (2006) (0.06 ddt/km^2/a northern hemisphere, 0.6 ddt/km^2/a southern hemisphere), Balme et al. (2003) (0.81 ddt/km^2/a Argyre Planitia, 0.47 ddt/km^2/a Hellas Basin) and Cantor et al. (2006) (0.344 dd/km^2/a estimated from Amazonis Planitia, Figure 16 in Cantor et al. (2006)) were used for the frequency of dust devils (Table 3; dd: dust devils; ddt: dust devil tracks).

The computed dust-lifting values range between $2.13{*}10^{-9}$ to $6.40{*}10^{-1}$ kg/m^2/a. The smallest

values are obtained when using the very low dust-lifting rate provided by Cantor et al. (2006). These results are at least two orders of magnitude smaller than the results calculated with the other dust-lifting rates. But Cantor et al. (2006) provide the largest dataset (four Martian years) and a somewhat statistically significant dust devil distribution. The dust devil frequency of 0.344 dd/km^2/a, however, is only an estimation of the Amazonis Planitia region, displayed in Figure 16 in Cantor et al. (2006). Because most dust devils have been seen in this area, this frequency provides an upper limit, but it is less than most of the frequency values of regions of the other publications. Results at the upper limit of dust-lifting rates between $2.13*10^{-3}$ and $6.40*10^{-1}$ kg/m^2/a are obtained when using the laboratory dust flux of $1*10^{-3}$ kg/m^2/s. But these values are in the range of the calculations using the dust flux from the Pathfinder site.

A preference can be given to the dust-lifting rates obtained with the dust fluxes derived from Spirit and Pathfinder data because these values can be regarded as field measurements. The travel distance as the interaction area is more reliable than the dust devil area alone because dust devils are naturally always moving. The dust devil frequencies are obtained investigating certain regions, but the values of Whelley and Greeley (2006) are averaged from several regions for each hemisphere and seem to provide more rigorous frequency values. The preferred values are $9.48*10^{-4}$ (northern hemisphere) and $9.48*10^{-3}$ kg/m^2/a (southern hemisphere), and $2.37*10^{-2}$ (northern hemisphere) and $2.37*10^{-1}$ kg/m^2/a (southern hemisphere) for Spirit and Pathfinder dust fluxes, respectively (Table 3).

The frequencies of dust devils are obtained from analyzing different regions and the dust-lifting rates are therefore only significant for the respective region and for the used typical dust devil diameter and the travel distance. Because the regions are known to show a higher dust devil activity, the dust-lifting rates may provide an upper limit compared to other regions on Mars. The more frequent but smaller dust devils are not included; it is also no global estimation for Mars. Including these facts would raise the amount of lifted dust again. But it can be seen

that the larger dust devils alone can contribute significantly to the atmospheric dust.

3.1.6 Joint observations

Joint HRSC and Spirit observations were done in October 2005 and April 2007. During the first observation campaign (∼1230 hours local time, southern summer) Spirit was able to image some dust devils, but they are not in the field of view of the HRSC images. The second attempt did also not reveal dust devils, neither by Spirit nor HRSC. The SRC was this time also used but showed no evidence of dust devil activity. The observations were done at late afternoon (∼1630 hours, southern spring) where the tendency for dust devils to form is much reduced compared to early afternoon.

3.2 HRSC versus MOC data

Next, we compared our data with results obtained from MOC image analyses (Whelley and Greeley, 2006; Fisher et al., 2005; Cantor et al., 2006). MOC provides a large database with over 200,000 images. The NA images allow detailed studies with their resolution of a few meters per pixel; the WA images offer the possibility to detect huge dust devils and to study their environment. Interannual investigations are possible due to the almost four Mars years the image data covers. But MOC observations are limited to afternoon hours between 1300-1500 hours due to the polar orbit of MGS. A dust devil is only imaged once by MOC, whereas HRSC provides additionally the translational speed, the direction of motion and the lifetime of dust devils.

3.2.1 Season

HRSC imaged dust devils in all seasons on both hemispheres, with most seen in spring (northern hemisphere) and summer (southern hemisphere) (Figure 2). The theoretical dust devil 'season' should be summer for both hemispheres. This cannot be approved from our northern

hemisphere data so far, probably due to the lack of dust devil detections. Cantor et al. (2006) reported an exception in dust devil occurrence between L_s=202.8°-281.5° in the north. They related this to increased regional dust storm activity and reduced solar heating. This explanation can be supported from our data, because we observed in four orbits on the northern hemisphere dust devil activity towards the end of the above mentioned period. Summarizing the regions and the seasons when dust devils have been observed, our data supports the hypothesis that dust devils evolve wherever the atmospheric conditions are suitable (Cantor et al., 2006).

3.2.2 Spatial coverage: active dust devils and tracks

Whelley and Greeley (2006) found a dust devil 'season', similar to results of Malin and Edgett (2001) and Cantor et al. (2006). However, Whelley and Greeley (2006) stated that the frequency of tracks in the southern hemisphere is an order of magnitude larger, which was attributed to differences in heating due to orbital asymmetries. The highest frequency was between 50° and 60°S latitude, consistent with our HRSC data (70 of 205 dust devils or 34% seen in this latitude range). This is in contrast to Cantor et al. (2006), who found in MOC images over 88% of about 11500 active dust devils in the northern hemisphere (most in Amazonis Planitia). Fisher et al. (2005) characterized Amazonis Planitia as the most active dust devil region planet wide as well. So far a total of 87 HRSC orbits (January 2004 July 2006) covering Amazonis Planitia were examined, including all seasons and ranging in local time from morning to late afternoon. Only six dust devils were detected in two orbits (1258 and 3042). No special remark is made about numerous occurrences between 50° and 60°S latitude by Cantor et al. (2006).

HRSC-observed dust devil tracks were only seen in those five orbits (from a total of 23 orbits with active dust devils) that cover the 50° to 60°S latitude range. This strengthens the argument of Whelley and Greeley (2006) that asymmetries in dust deposits are responsible for the

paucity of tracks in the northern hemisphere in comparison to the southern hemisphere (Figure 6). Only seven dust devils were observed creating tracks; usually either active dust devils or tracks are seen. This is in agreement with Fisher et al. (2005), who observed in Casius and Utopia Planitia no single active dust devil, but many tracks.

The highest dust devil track frequency is found in the northern hemisphere between 60° and 70°N, as seen in MOC images (Whelley and Greeley, 2006). This was not observed in HRSC data, as no active dust devils were seen north of 43°N. Most dust devils in the northern hemisphere were detected in the southern parts of Chryse Planitia. Fisher et al. (2005) detected three active dust devils (local winter) and four dust devil tracks (local summer and winter) in this region. Metzger et al. (1999) and Ferri et al. (2003) showed using Mars Pathfinder lander images that this is an active dust devil region. Taking these results and those from Whelley and Greeley (2006) in account, there is a possible explanation for the high number of active dust devils seen in southern Chryse Planitia. It is a region of higher surface pressure (lowland) with a thick dust layer which favors dust devil formation. In addition, there is maybe a flow field induced by the valley system (Valles Marineris disembogues into Simud Vallis and Simud Vallis finally into Chryse Planitia) and the surrounded highlands that forces dust devil formation.

5. Conclusion

Observations of dust devils from orbit complement those seen from the surface. Spirit and Pathfinder imaged smaller dust devils and provide insight into details such as formation, frequency, vertical velocity and dust flux. Statistics can be assembled for the daily and seasonal distribution of dust devils at the landing site. The tracks of dust devils can be studied in order to examine the particles that have been removed and injected into the atmosphere.

Lander observations, however, are restricted to a single location and generally one viewing direction per sol (Greeley et al., 2006). HRSC provides three years of nearly global coverage

of the Martian surface. From its field of view, more and larger dust devils can be detected simultaneously in HRSC data. A reliable size of larger dust devils can only be retrieved by orbiter images. This includes the upper size limits of dust devils.

The local time when dust devils are imaged, the translational speed and the lifetime of dust devils agree favorably when comparing orbiter with lander data.

After the analysis of almost 200 dust devil speeds it can be concluded that dust devils move with the ambient wind as it always was expected. The derived dust devil speeds can therefore be taken as an indirect measurement of the surface wind speeds. The analysis of the directions of motion of the dust devils in southern Chryse Planitia and Peneus Patera show the expected behavior by moving with the general circulation (Hadley circulation).

The results from Whelley and Greeley (2006) can be confirmed with the high dust devil activity seen in HRSC images between 50° and 60°S latitude. The abundance of dust devils in Amazonis Planitia seen by Fisher et al. (2005) and Cantor et al. (2006) cannot be verified by HRSC data.

The results of the dust-lifting rate calculations suggest that large dust devils alone can contribute significantly to the atmospheric haze and provide their contribution to the global dust settling rate of $2*10^{-2}$ kg/m^2/a (Pollack et al., 1979). Judging from the capability of dust devils to lift and move dust to a large extent, dust devils are definitely responsible for local redistributions of dust and sand, depending on their forward speed, direction of motion and lifetime. Hadley circulation, which is stronger and wider during southern summer than northern summer, increases dust devil activity where the ascending branch is located. This is consistent with Whelley and Greeley (2006 and in press) and suggests a significant local dust transport from the 50° to 60°S latitude range where most dust devils have been seen in this study to south-eastern directions due to the trade winds associated with the Hadley circulation (confirmed by measured directions of motion).

Acknowledgements

This work was supported by the DFG, Bonn, under grant PA 525/4-3, within the scope of the priority program 'Mars and the Terrestrial Planets' and by DLR, Bonn-Oberkassel, under grant 50QM9909. The U.S. Investigations were supported by NASA through contracts to the Jet Propulsion Laboratory. We thank the HRSC Experiment Teams at DLR Berlin and Freie Universitaet Berlin as well as the Mars Express Project Teams at ESTEC and ESOC for their successful planning and acquisition of data as well as for making the processed data available to the HRSC Team. We acknowledge the effort of the HRSC Co-Investigator Team members and their associates who have contributed to this investigation in the preparatory phase and in scientific discussions within the Team.

References

Biener, K.K., Geissler, P. E., McEwen, A. S., Leovy, C. 2002. Observations of dust devils in MOC wide angle camera images. Lunar. Planet. Sci. XXXIII, abstract no. 2004.

Balme, M., Hagermann, A. 2006. Particle lifting at the soil-air interface by atmospheric pressure excursions in dust devils. Geophys. Res. Lett. 33, L19S01, doi:10.1029/2006GL026819.

Balme, M. R., Whelley, P. L., Greeley, R. 2003. Mars: Dust devil track survey in Argyre Planitia and Hellas Basin. J. Geophys. Res. 108(E8), 5086, doi:10.1029/2003JE002096.

Cantor, B. A., Malin, M., Edgett, K. S. 2002. Multiyear Mars Orbiter Camera (MOC) observations of repeated martian weather phenomena during the northern summer season. J. Geophys. Res. 107(E3), 5014, doi:10.1029/2001JE001588.

Cantor, B. A., Kanak, K. M., Edgett, K. S. 2006. Mars Orbiter Camera observations of Martian dust devils and their tracks (September 1997 to January 2006) and evaluation of theoretical vortex models. J. Geophys. Res. 111, E12002, doi:10.1029/2006JE002700.

Ferri, F., Smith, P. H., Lemmon, M., Rennó, N. O. 2003. Dust devils as observed by Mars Pathfinder, J. Geophys. Res. 108(E12), 5133, doi:10.1029/2000JE001421.

Fisher, J. A., Richardson, M. I., Newman, C. E., Szwast, M. A., Graf, C., Basu, S., Ewald, S. P., Toigo, A. D., Wilson, R. J. 2005. A survey of Martian dust devil activity using Mars Global Surveyor Mars Orbiter Camera images. J. Geophys. Res. 110, E03004, doi:10.1029/2003JE002165.

Gierasch, P. J., Goody, R. M. 1973. A model of a martian great dust storm. J. Atmos. Sci. 30, 169-179.

Greeley, R., Balme, M. R., Iversen, J. D., Metzger, S., Mickelson, R., Phoreman, J., White, B. 2003. Martian dust devils: Laboratory simulations of particle threshold. J. Geophys. Res. 108(E5), 5041, doi:10.1029/2002JE001987.

Greeley, R., Whelley, P. L., Neakrase, L. D. V. 2004. Martian dust devils: Directions of movement inferred from their tracks. Geophys. Res. Lett. 31, L24702, doi:10.1029/2004GL021599.

Greeley, R., 13 colleagues 2006. Active dust devils in Gusev Crater, Mars: Observations from the Mars Exploration Rover, Spirit. J. Geophys. Res. 111, E12S09, doi:10.1029/2006JE002743.

Ives, R. L. 1947. Behavior of Dust Devils. Bull. Am. Meteorol. Soc. 28, 168-174.

Kanak, K. M. 2006. On the numerical simulation of dust devil-like vortices in terrestrial and Martian convective boundary layers. Geophys. Res. Lett. 33, L19S05, doi:10.1029/2006GL026207.

Malin, M. C., Edgett, K. S. 2001. Mars Global Surveyor Mars Orbiter Camera: Interplanetary cruise through primary mission. J. Geophys. Res. 106(E10), 23,429-23,570.

Metzger, S. M. 2003. Promoting a well-established study site for Mars analog and desert process studies. Lunar Planet. Sci. XXXIV, abstract no. 2048.

Metzger, S. M., Carr, J. R., Johnson, J. R., Parker, T. J., Lemmon, M. T. 1999. Dust devil vortices seen by the Mars Pathfinder camera. Geophys. Res. Letters 26(18), 2781-2784.

Murphy, J. R., Nelli, S. 2002. Mars Pathfinder convective vortices: Frequency of occurrence. Geophys. Res. Lett. 29(23), 2103, doi:10.1029/2002GL015214.

Neakrase, L. D. V., Greeley, R., Iversen, J. D., Balme, M. R., Eddlemon, E. E. 2006. Dust flux within dust devils: Preliminary laboratory simulations. Geophys. Res. Lett. 33, L19S09, doi:10.1029/2006GL026810.

Neubauer, F. M. 1966. Thermal convection in the Martian atmosphere. J. Geophys. Res. 71, 2419-2426.

Oberst, J., 16 colleagues. 2008. The imaging performance of the SRC on Mars Express. Plan-

etary and Space Science 56, 473-491.

Rennó, N. O., Bluestein, H. B. 2001. A Simple Theory of Waterspouts. J. Atmos. Sci. 58, 927-932.

Rennó, N. O., Burkett, M. L., Larkin, M. P. 1998. A simple thermodynamical theory for Dust Devils. J. Atmos. Sci. 55, 3244-3252.

Rennó, N. O., Nash, A. A., Lunine, J., Murphy, J. 2000. Martian and terrestrial dust devils: Test of a scaling theory using Pathfinder data. J. Geophys. Res. 105(E1), 1859-1865.

Ringrose, T. J., Towner, M. C., Zarnecki, J. C. 2003. Convective vortices on Mars: a reanalysis of Viking Lander 2 meteorological data, sols 1-60. Icarus 163, 78-87.

Ryan, J. A. 1964. Notes on the Martian yellow clouds. J. Geophys. Res. 69, 3759-3770.

Ryan, J. A. 1972. Relation of Dust Devil Frequency and Diameter to Atmospheric Temperature. J. Geophys. Res. 77, No. 36, 7133-7137.

Ryan, J. A., Lucich, R. D. 1983. Possible Dust Devils, Vortices on Mars. J. Geophys. Res. 88(C15), 11005-11011.

Sinclair, P. C. 1969. General Characteristics of Dust Devils. J. Appl. Meteorol. 8, 32-45.

Snow, J. T., McClelland, T. M. 1990. Dust Devils at White Sands Missile Range, New Mexico,

1. Temporal and Spatial Distributions. J. Geophys. Res. 95(D9), 13707-13721.

Stanzel, C., Pätzold, M., Greeley, R., Hauber, E., Neukum, G. 2006. Dust devils on Mars observed by the High Resolution Stereo Camera. Geophys. Res. Lett. 33, L11202, doi:10.1029/2006GL025816.

Thomas, P., Gierasch, P. J. 1985. Dust devils on Mars. Science 230, 175-177.

Toigo, A. D., Richardson, M. I., Ewald, S. P., Gierasch, P. J. 2003. Numerical simulation of Martian dust devils. J. Geophys. Res. 108(E6), 5047, doi:10.1029/2002JE002002.

Wennmacher, A., Neubauer, F. M., Pätzold, M., Schmitt, J., Schulte, K. 1996. A Search for Dust Devils on Mars. Lunar. Planet. Sci. XXVII, 1417 (abstract).

Whelley, P. L., Greeley, R. 2006. Latitudinal dependency in dust devil activity on Mars. J. Geophys. Res. 111, E10003, doi:10.1029/2006JE002677.

Whelley, P. L., Greeley, R. 2008. The Distribution of Dust Devil Activity on Mars. J. Geophys. Res. doi: 10.1029/2007JE002966, in press.

Zurek, R. W., Barnes, J. R., Haberle, R. M., Pollack, J. B., Tillman, J. E., Leovy, C. B. 1992. Dynamics of the atmosphere of Mars. In: Kieffer, H. H., Jakosky, B. M., Snyder, C., Matthews, M. S. (Eds.), Mars. Univ. of Ariz. Press, Tucson, pp. 835-933.

Table 1

Dust Devil Characteristics. S1 represents the forward looking channel, ND the nadir, and S2 the backward looking channel. LT stands for the local time.

Dust Devil Number	S1-ND, m/s	ND-S2, m/s	Diameter, m	Height, m
Arcadia Dorsa / Arcadia Planitia, Image = h0037_0000, $L_s = 337°$*, LT = 14:15, Lat = 43° N, Lon = 230° E*				
dust devil 1	-	23.3 ± 1.3	168 ± 63	490 ± 96
dust devil 2	-	24.3 ± 1.4	265 ± 63	615 ± 98
dust devil 3	-	24.6 ± 1.3	361 ± 63	275 ± 97
Icaria Planum, Image = h0068_0000, $L_s = 343°$*, LT = 13:25, Lat = 40° S, Lon = 255° E*				
dust devil 1	-	14.8 ± 3.8	159 ± 63	386 ± 234
Syrtis Planum, Image = h1054_0000, $L_s = 115°$*, LT = 15:03, Lat = 1° S, Lon = 70° E*				
dust devil 1	26.8 ± 7.3	21.4 ± 7.1	313 ± 63	-
Thaumasia Planum, Image = h1081_0000, $L_s = 118°$*, LT = 14:55, Lat = 23° S, Lon = 297° E*				
dust devil 1	-	20.8 ± 3.4	138 ± 63	649 ± 95
dust devil 2	22.7 ± 4.0	18.8 ± 3.4	205 ± 63	2474 ± 95
dust devil 3	20.0 ± 4.0	15.0 ± 3.3	654 ± 63	2956 ± 94
dust devil 4	21.4 ± 4.0	17.8 ± 3.3	230 ± 63	3371 ± 94
dust devil 5	16.8 ± 4.0	16.9 ± 3.3	158 ± 63	410 ± 94
Amazonis Planitia, Image = h1258_0001, $L_s = 142°$*, LT = 12:44, Lat = 34° N, Lon = 182° E*				
dust devil 1	2.2 ± 6.3	6.0 ± 6.1	50 ± 63	1043 ± 444
dust devil 2	3.2 ± 6.3	1.8 ± 6.1	88 ± 63	984 ± 452
dust devil 3	1.6 ± 6.2	1.5 ± 6.0	73 ± 63	1277 ± 453
dust devil 4	5.8 ± 6.2	2.7 ± 5.9	50 ± 63	1399 ± 470
dust devil 5	5.6 ± 6.2	5.1 ± 6.0	100 ± 63	919 ± 471
Arcadia Dorsa / Arcadia Planitia, Image = h1404_0001, $L_s = 163°$*, LT = 11:10, Lat = 44° N, Lon = 230° E*				
dust devil 1	18.0 ± 4.2	18.6 ± 4.7	95 ± 63	226 ± 226
dust devil 2	22.7 ± 4.1	21.9 ± 4.7	253 ± 63	2108 ± 230
Hydraotes Chaos, Image = h2024_0001, $L_s = 267°$*, LT = 15:44, Lat = 0° S, Lon = 326° E*				
dust devil 1	13.1 ± 6.7	19.5 ± 6.6	278 ± 63	467 ± 105
Syria Planum, Image = h2032_0000, $L_s = 269°$*, LT = 15:30, Lat = 10° S, Lon = 258° E*				
dust devil 1	24.6 ± 6.6	22.9 ± 6.2	138 ± 63	2059 ± 138
dust devil 2	16.8 ± 6.6	17.0 ± 6.2	80 ± 63	109 ± 138
Simud Vallis, Image = h2035_0000, $L_s = 269°$*, LT = 15:34, Lat = 8° N, Lon = 324° E*				
dust devil 1	23.1 ± 6.0	24.5 ± 6.3	125 ± 63	327 ± 84
dust devil 2	25.2 ± 6.2	24.8 ± 6.5	115 ± 63	298 ± 90
dust devil 3	31.4 ± 6.3	18.7 ± 6.5	146 ± 63	216 ± 91
dust devil 4	30.9 ± 6.3	-	45 ± 63	75 ± 91
dust devil 5	-	-	372 ± 125	443 ± 191
dust devil 6	27.1 ± 6.4	25.5 ± 6.7	177 ± 63	289 ± 95

Dust Devil Number	S1-ND, m/s	ND-S2, m/s	Diameter, m	Height, m
dust devil 7	24.6 ± 6.4	16.8 ± 6.6	188 ± 63	237 ± 95
dust devil 8	37.4 ± 6.5	34.8 ± 6.7	160 ± 63	521 ± 96
dust devil 9	22.8 ± 6.5	25.8 ± 6.7	229 ± 63	628 ± 97
dust devil 10	22.4 ± 6.6	26.1 ± 6.8	426 ± 63	-
dust devil 11	26.4 ± 6.9	21.4 ± 6.7	208 ± 63	282 ± 101
dust devil 12	20.1 ± 6.6	21.4 ± 7.0	185 ± 63	606 ± 101
dust devil 13	24.2 ± 6.6	16.8 ± 6.7	80 ± 63	195 ± 101
dust devil 14	17.3 ± 6.6	24.6 ± 6.8	180 ± 63	780 ± 101
dust devil 15	26.8 ± 6.7	22.6 ± 6.8	226 ± 63	704 ± 102
dust devil 16	23.3 ± 6.7	25.3 ± 6.8	118 ± 63	384 ± 103
dust devil 17	31.8 ± 6.8	23.1 ± 6.8	80 ± 63	527 ± 103
dust devil 18	47.8 ± 6.8	54.0 ± 6.9	636 ± 63	-
dust devil 19	31.4 ± 6.8	36.3 ± 6.9	186 ± 63	526 ± 105
dust devil 20	41.7 ± 6.6	35.4 ± 6.6	80 ± 63	468 ± 125
Xanthe Dorsa (Chryse Planitia) / Simud Vallis, Image = h2046_0000, $L_s = 271°$*, LT = 15:25, Lat = 14° N, Lon = 323° E*				
dust devil 1	-	59.1 ± 5.8	425 ± 63	-
dust devil 2	-	-	119 ± 63	136 ± 82
dust devil 3	-	31.2 ± 5.8	84 ± 63	147 ± 84
dust devil 4	-	23.9 ± 5.8	289 ± 63	-
dust devil 5	25.1 ± 5.6	27.8 ± 6.0	125 ± 63	369 ± 88
dust devil 6	21.9 ± 5.6	30.3 ± 6.0	106 ± 63	134 ± 89
dust devil 7	31.2 ± 5.6	30.6 ± 6.0	90 ± 63	87 ± 89
dust devil 8	20.9 ± 5.6	-	278 ± 63	729 ± 90
dust devil 9	24.1 ± 5.8	-	151 ± 63	264 ± 93
dust devil 10	21.6 ± 5.8	-	258 ± 63	1744 ± 93
dust devil 11	20.7 ± 5.8	-	113 ± 63	2835 ± 93
Syria Planum, Image = h2054_0000, $L_s = 273°$*, LT = 15:13, Lat = 10° S, Lon = 258° E*				
dust devil 1	43.9 ± 7.2	16.7 ± 6.7	1648 ± 63	4437 ± 156
dust devil 2	19.4 ± 7.0	23.1 ± 6.7	361 ± 63	547 ± 157
dust devil 3	20.1 ± 7.0	16.7 ± 6.7	133 ± 63	1060 ± 157
dust devil 4	18.4 ± 7.0	22.0 ± 6.7	335 ± 63	694 ± 157
dust devil 5	24.0 ± 7.0	24.9 ± 6.7	1433 ± 63	1882 ± 157
Xanthe Terra / Vallis Marineris, Image = h2090_0000, $L_s = 279°$*, LT = 14:41, Lat = 10° N / -13° S, Lon = 319° E*				
dust devil 1	10.8 ± 5.1	22.0 ± 5.6	133 ± 63	331 ± 134
dust devil 2	18.1 ± 5.2	22.1 ± 5.7	106 ± 63	615 ± 134
dust devil 3	15.3 ± 7.0	19.1 ± 6.9	221 ± 63	1503 ± 209
dust devil 4	22.7 ± 6.9	25.0 ± 6.7	186 ± 63	398 ± 224
Peneus Patera, Image = h2100_0000, $L_s = 281°$*, LT = 14:15, Lat = 57° S, Lon = 56° E*				
dust devil 1	11.8 ± 4.4	11.2 ± 3.1	285 ± 125	2665 ± 396
dust devil 2	11.5 ± 5.4	12.1 ± 4.0	280 ± 125	476 ± 439
dust devil 3	13.0 ± 5.2	12.7 ± 3.9	309 ± 125	812 ± 435
dust devil 4	1.5 ± 4.9	2.5 ± 3.6	226 ± 125	122 ± 419
dust devil 5	11.5 ± 4.9	15.0 ± 3.6	351 ± 125	232 ± 421
dust devil 6	10.8 ± 5.6	8.0 ± 4.2	361 ± 125	605 ± 448
dust devil 7	13.6 ± 5.1	11.2 ± 3.8	430 ± 125	1473 ± 431
dust devil 8	14.7 ± 5.1	15.1 ± 3.8	426 ± 125	463 ± 429

Dust Devil Number	S1-ND, m/s	ND-S2, m/s	Diameter, m	Height, m
dust devil 9	13.3 ± 5.1	12.6 ± 3.8	426 ± 125	497 ± 428
dust devil 10	10.2 ± 4.8	14.6 ± 3.5	354 ± 125	355 ± 416
dust devil 11	-	17.0 ± 3.6	302 ± 125	972 ± 415
dust devil 12	-	7.5 ± 2.8	382 ± 125	412 ± 375
dust devil 13	-	9.3 ± 2.9	301 ± 125	459 ± 382
dust devil 14	7.7 ± 5.3	10.4 ± 4.0	355 ± 125	433 ± 436
dust devil 15	15.3 ± 5.2	13.2 ± 3.9	407 ± 125	665 ± 435
dust devil 16	15.0 ± 5.2	8.4 ± 3.9	318 ± 125	1034 ± 432
dust devil 17	-	12.4 ± 3.8	266 ± 125	809 ± 430
dust devil 18	-	-	195 ± 125	327 ± 406
dust devil 19	9.9 ± 4.6	-	305 ± 125	372 ± 405
dust devil 20	8.1 ± 4.1	9.3 ± 2.8	372 ± 125	387 ± 380
dust devil 21	-	-	472 ± 125	562 ± 374
dust devil 22	11.9 ± 4.1	9.8 ± 2.8	340 ± 125	511 ± 378
dust devil 23	14.5 ± 4.1	12.5 ± 2.8	391 ± 125	657 ± 378
dust devil 24	-	5.5 ± 2.8	301 ± 125	210 ± 380
dust devil 25	-	-	247 ± 125	639 ± 374
dust devil 26	11.0 ± 5.2	7.3 ± 3.9	401 ± 125	880 ± 432
Xanthe Terra / Eos Mensa (Valles Marineris), Image = h2101_0000, $L_s = 281°$*, LT = 14:32, Lat = 8° N / 10° S, Lon = 319° E*				
dust devil 1	17.8 ± 4.6	18.9 ± 5.0	98 ± 63	315 ± 131
dust devil 2	12.5 ± 4.4	13.7 ± 5.0	125 ± 63	289 ± 132
dust devil 3	13.3 ± 4.4	16.4 ± 5.0	98 ± 63	563 ± 132
dust devil 4	14.4 ± 4.4	17.9 ± 5.0	157 ± 63	694 ± 132
dust devil 5	14.7 ± 4.4	17.1 ± 5.0	135 ± 63	255 ± 133
dust devil 6	18.9 ± 5.2	21.8 ± 5.7	195 ± 63	1686 ± 150
dust devil 7	19.0 ± 5.6	31.9 ± 6.1	256± 63	835 ± 160
dust devil 8	4.0 ± 6.8	2.1 ± 6.9	1008 ± 63	2208 ± 207
dust devil 9	19.1 ± 6.9	14.2 ± 7.1	143 ± 63	705 ± 208
dust devil 10	14.5 ± 7.0	26.2 ± 7.0	654 ± 63	1107 ± 220
dust devil 11	3.9 ± 6.6	6.7 ± 7.1	108 ± 63	383 ± 233
Xanthe Terra / Noachis Terra, Image = h2112_0000, $L_s = 283°$*, LT = 14:22, Lat = 10° N / 20° S, Lon = 318° E*				
dust devil 1	19.3 ± 4.2	17.7 ± 4.8	67 ± 63	174 ± 141
dust devil 2	16.4 ± 4.4	19.5 ± 4.9	174 ± 63	543 ± 147
dust devil 3	18.0 ± 4.4	19.3 ± 5.0	124 ± 63	426 ± 147
dust devil 4	16.3 ± 5.4	19.9 ± 5.8	98 ± 63	183 ± 173
dust devil 5	17.1 ± 5.7	19.4 ± 6.1	138 ± 63	1071 ± 181
dust devil 6	16.4 ± 5.7	23.0 ± 6.2	246 ± 63	1523 ± 184
dust devil 7	13.1 ± 6.7	10.8 ± 6.1	141 ± 63	500 ± 224
dust devil 8	9.6 ± 7.0	14.5 ± 6.7	354 ± 63	1379 ± 279
Peneus Patera, Image = h2133_0000, $L_s = 287°$*, LT = 13:40, Lat = 58° S, Lon = 53° E*				
dust devil 1	22.3 ± 5.8	13.0 ±4.5	255 ± 125	1322 ± 447
dust devil 2	8.6 ± 5.6	8.7 ± 4.3	202 ± 125	571 ± 438
dust devil 3	12.1 ± 5.5	6.9 ± 4.2	90 ± 125	1352 ± 433
dust devil 4	-	-	250 ± 250	1293 ± 784
dust devil 5	8.8 ± 6.4	7.9 ± 5.1	283 ± 125	1043 ± 479
dust devil 6	19.2 ± 6.2	16.8 ± 4.8	305 ± 125	539 ± 468
Noachis Terra, Image = h2225_0000,				

Dust Devil Number	S1-ND, m/s	ND-S2, m/s	Diameter, m	Height, m
L_s = 302°, LT = 12:30, Lat = 52°S, Lon = 14°E				
dust devil 1	-	12.3 ±5.1	138 ± 63	1242 ± 283
dust devil 2	-	4.7 ± 4.0	188 ± 63	479 ± 223
dust devil 3	-	5.1 ± 3.8	188 ± 63	263 ± 212
dust devil 4	-	7.0 ± 3.8	138 ± 63	-
dust devil 5	-	3.8 ± 3.8	126 ± 63	228 ± 211
dust devil 6	-	8.7 ± 3.8	175 ± 63	272 ± 212
dust devil 7	-	8.2 ± 4.1	234 ± 63	555 ± 229
dust devil 8	-	8.5 ± 4.1	289 ± 63	998 ± 229
Terra Cimmeria, Image = h2242_0000, L_s = 305°, LT = 12:20, Lat = 56°S, Lon = 143°E				
dust devil 1	-	5.4 ±5.6	388 ± 63	912 ± 286
dust devil 2	3.9 ± 7.2	2.9 ± 5.7	313 ± 63	1508 ± 289
dust devil 3	6.6 ± 7.2	5.6 ± 5.7	113 ± 63	426 ± 288
dust devil 4	2.1 ± 6.1	3.1 ± 5.6	155 ± 63	383 ± 282
dust devil 5	-	4.5 ± 4.4	143 ± 63	335 ± 282
dust devil 6	-	5.0 ± 5.6	250 ± 63	395 ± 283
dust devil 7	6.4 ± 6.1	10.9 ± 5.5	138 ± 63	302 ± 281
dust devil 8	-	-	126 ± 63	242 ± 280
dust devil 9	-	-	258 ± 63	473 ± 242
dust devil 10	-	-	316 ± 63	1045 ± 241
dust devil 11	-	3.0 ± 4.5	213 ± 63	546 ± 224
dust devil 12	-	4.5 ± 4.3	200 ± 63	477 ± 213
dust devil 13	-	3.7 ± 4.2	127 ± 63	243 ± 210
dust devil 14	-	5.5 ± 4.1	200 ± 63	282 ± 202
dust devil 15	-	6.9 ± 4.1	151 ± 63	319 ± 202
dust devil 16	5.7 ± 4.7	5.6 ± 4.1	198 ± 63	222 ± 201
dust devil 17	-	10.7 ± 4.2	131 ± 63	256 ± 201
dust devil 18	-	5.5 ± 5.0	125 ± 63	322 ± 248
dust devil 19	-	5.1 ± 5.0	168 ± 63	322 ± 248
dust devil 20	-	3.2 ± 5.0	143 ± 63	374 ± 245
dust devil 21	-	5.7 ± 4.0	223 ± 63	267 ± 207
dust devil 22	-	-	195 ± 63	340 ± 244
dust devil 23	3.7 ± 5.5	3.8 ± 4.9	230 ± 63	981 ± 244
dust devil 24	-	2.0 ± 4.9	221 ± 63	301 ± 243
dust devil 25	5.1 ± 5.2	4.4 ± 4.6	170 ± 63	408 ± 226
dust devil 26	8.0 ± 4.8	6.7 ± 4.1	129 ± 63	147 ± 202
Terra Cimmeria, Image = h2315_0000, L_s = 317°, LT = 11:20, Lat = 57°S, Lon = 170°E				
dust devil 1	5.4 ±6.7	-	50 ± 63	145 ± 204
dust devil 2	8.3 ±6.7	-	163 ± 63	284 ± 204
dust devil 3	8.1 ±6.7	-	331 ± 63	746 ± 203
dust devil 4	12.7 ±6.5	-	168 ± 63	295 ± 193
Amazonis Planitia, Image = h3042_0000, L_s = 57°, LT = 16:25, Lat = 23°N, Lon = 206°E				
dust devil 1	-	-	151 ± 63	104 ± 101
Xanthe Dorsa (Chryse Planitia), Image = h3202_0000, L_s = 76°, LT = 14:47, Lat = 19°N, Lon = 323°E				
dust devil 1	2.3 ± 6.2	2.2 ± 6.0	75 ± 63	580 ± 218
dust devil 2	4.3 ± 6.0	4.4 ± 5.7	118 ± 63	1210 ± 209

Dust Devil Number	S1-ND, m/s	ND-S2, m/s	Diameter, m	Height, m
dust devil 3	5.1 ± 6.1	3.5 ± 5.8	416 ± 63	1187 ± 215
dust devil 4	2.5 ± 6.2	8.2 ± 6.0	416 ± 63	1324 ± 214
dust devil 5	4.8 ± 6.2	6.3 ± 5.9	319 ± 63	1103 ± 214
Syria Planum, Image = h3210_0000, L_s = 77°, LT = 14:50, Lat = 10°S, Lon = 257°E				
dust devil 1	15.9± 3.3	16.9± 2.6	327 ± 63	1155 ± 129
Xanthe Dorsa (Chryse Planitia), Image = h3246_0000, L_s = 82°, LT = 14:20, Lat = 17°N, Lon = 317°E				
dust devil 1	4.3± 5.6	3.7± 5.2	151 ± 63	993 ± 281
dust devil 2	9.7± 5.6	9.8± 5.2	146 ± 63	284 ± 280
dust devil 3	7.8± 5.6	8.3± 5.2	64 ± 63	160 ± 281
dust devil 4	4.7± 5.5	6.7± 5.1	91 ± 63	243 ± 278
dust devil 5	6.4± 5.5	2.3± 5.1	143 ± 63	591 ± 278
dust devil 6	7.9± 5.5	4.4± 5.1	125 ± 63	329 ± 278
dust devil 7	15.1± 5.6	8.6± 5.1	222 ± 63	835 ± 277
dust devil 8	6.9± 5.5	2.2± 5.1	125 ± 63	670 ± 277
dust devil 9	6.4± 6.9	6.2± 4.3	302 ± 63	795 ± 280
dust devil 10	8.0± 5.5	8.9± 5.1	248 ± 63	644 ± 275
dust devil 11	2.4± 5.3	4.8± 5.0	108 ± 63	321 ± 275
dust devil 12	5.2± 5.4	8.2± 5.0	202 ± 63	737 ± 274
dust devil 13	7.2± 5.4	8.2± 5.0	219 ± 63	295 ± 274
dust devil 14	5.4± 5.5	7.5± 5.0	115 ± 63	258 ± 274
dust devil 15	6.9± 5.4	4.6± 5.0	135 ± 63	387 ± 273
dust devil 16	8.6± 5.4	7.3± 5.0	266 ± 63	384 ± 273
dust devil 17	3.9± 5.4	5.0± 5.0	178 ± 63	405 ± 273
dust devil 18	2.9± 5.5	6.0± 5.0	223 ± 63	469 ± 274
dust devil 19	2.7± 5.5	5.8± 5.0	146 ± 63	216 ± 274
dust devil 20	5.2± 5.5	5.3± 5.0	71 ± 63	156 ± 274
dust devil 21	3.9± 5.5	6.6± 5.0	101 ± 63	251 ± 273
dust devil 22	-	3.2± 4.9	205 ± 63	389 ± 272
dust devil 23	5.8± 5.4	4.0± 5.0	98 ± 63	219 ± 272
dust devil 24	9.2± 5.4	11.6± 4.9	168 ± 63	463 ± 270
dust devil 25	5.4± 5.4	8.7± 4.9	95 ± 63	135 ± 270
dust devil 26	6.5± 5.4	5.7± 4.9	118 ± 63	361 ± 270
dust devil 27	5.8± 5.4	9.5± 4.9	355 ± 63	666 ± 271
dust devil 28	6.1± 5.4	3.9± 4.9	141 ± 63	288 ± 271
dust devil 29	8.8± 5.4	11.1± 4.9	170 ± 63	302 ± 270
dust devil 30	8.2± 5.4	7.0± 4.9	178 ± 63	260 ± 270
dust devil 31	6.8± 5.2	13.0± 4.7	281 ± 63	889 ± 263
dust devil 32	10.7± 5.0	10.1± 4.5	153 ± 63	236 ± 254
dust devil 33	12.2± 5.0	13.5± 4.4	135 ± 63	238 ± 252
dust devil 34	10.4± 4.9	13.8± 4.4	115 ± 63	176 ± 251
dust devil 35	11.3± 5.7	6.9± 5.3	531 ± 63	2228 ± 283
dust devil 36	0.9± 5.7	4.7± 5.3	203 ± 63	422 ± 283
dust devil 37	5.7± 5.6	5.8± 5.2	141 ± 63	457 ± 280
dust devil 38	8.9± 5.5	5.9± 4.9	143 ± 63	244 ± 276
dust devil 39	1.9± 5.5	4.3± 5.1	141 ± 63	552 ± 276
dust devil 40	6.9± 5.5	4.3± 5.1	186 ± 63	345 ± 276
dust devil 41	13.3± 5.4	7.4± 4.9	125 ± 63	238 ± 267
dust devil 42	7.6± 5.4	3.7± 4.9	106 ± 63	229 ± 269
dust devil 43	8.2± 5.3	6.6± 4.8	186 ± 63	729 ± 267

Dust Devil Number	S1-ND, m/s	ND-S2, m/s	Diameter, m	Height, m
dust devil 44	10.3± 5.3	7.9± 4.8	221 ± 63	574 ± 266
dust devil 45	9.8± 5.3	10.3± 4.8	168 ± 63	187 ± 265
dust devil 46	9.0± 5.1	10.5± 4.6	141 ± 63	112 ± 260
dust devil 47	9.9± 5.1	12.4± 4.6	160 ± 63	256 ± 260
dust devil 48	10.9± 5.1	11.1± 4.6	151 ± 63	370 ± 259
dust devil 49	6.3± 5.0	6.0± 4.5	292 ± 63	742 ± 256

Table 2

Comparison between HRSC and Spirit/Pathfinder observations (DD = dust devils).

Dust devil Feature	**HRSC (205 dust devils)**	**Spirit (Gusev crater, 533 dust devils)**	**Pathfinder (Chryse Planitia) 5 dust devils: Metzger et al. (1999) / 14 dust devils: Ferri et al. (2003)**
Location (Hemisphere)	12°-44°N; mostly 10°-20°N 1°-62°S; mostly 50°-60°S	14°S	19°N
Local Time	1110-1630 hours	0930-1630 hours	1130-1250 hrs / 1120-1510 hrs
Solar Longitude	57°-337° L_s (N) 77°-343° L_s (S)	173°-340° L_s (S)	148° L_s (N) / 143° + 148° L_s (N)
Height	75-4440 m mostly <1000 m	10-360 m (full range) up to 850 m (truncated)	46-350 m / -
Diameter	45-1650 m mostly <400 m	2-280 m mostly 10-20 m	14-79 m / 11-573 m - / mostly 100-200 m
Traverse speed	1-59 m/s mostly <15 m/s	<1-21 m/s	0.5-4.6 m/s / 10 m/s
Lifetime	3.7-32.5 min (12 DD minimum lifetime) mean 13 min	0.7-11.5 min (59 DD full cycle) 0.3-32.3 min (290 DD minimum lifetime); mean 2.8 min	-
Dust Lifting Rate	9.39×10^{-4} - 2.35×10^{-1} kg/m^2/a (preferred values)	1.3×10^{-2} kg/m^2/a	-

Table 3

Estimations of dust lifting rates. Mean dust devil duration is 790 s. 'dd' stands for dust devils, 'ddt' stands for dust devil tracks. More details in the text.

Source	Dust Flux ($kg/m^2/s$)	Area (m^2)	Number dust devils ($dd(t)/km^2/a$)	Dust Lifting Rate ($kg/m^2/a$)
Spirit (Greeley et al., 2006)	2×10^{-5}	4.2×10^{4}	0.060	3.98×10^{-5}
			0.600	3.98×10^{-4}
			0.810	5.38×10^{-4}
			0.470	3.12×10^{-4}
			0.344	2.28×10^{-4}
		9.9×10^{5}	0.060	9.39×10^{-4}
			0.600	9.39×10^{-3}
			0.810	1.27×10^{-2}
			0.470	7.35×10^{-3}
			0.344	5.38×10^{-3}
Mars Pathfinder (Metzger et al., 1999)	5×10^{-4}	4.2×10^{4}	0.060	9.95×10^{-4}
			0.600	9.95×10^{-3}
			0.810	1.34×10^{-2}
			0.470	7.80×10^{-3}
			0.344	5.71×10^{-3}
		9.9×10^{5}	0.060	2.35×10^{-2}
			0.600	2.35×10^{-1}
			0.810	3.17×10^{-1}
			0.470	1.84×10^{-1}
			0.344	1.35×10^{-1}
MOC (Cantor et al., 2006)	1×10^{-9}	4.2×10^{4}	0.060	1.99×10^{-9}
			0.600	1.99×10^{-8}
			0.810	2.69×10^{-8}
			0.470	1.56×10^{-8}
			0.344	1.14×10^{-8}
		9.9×10^{5}	0.060	4.69×10^{-8}
			0.600	4.69×10^{-7}
			0.810	6.34×10^{-7}
			0.470	3.68×10^{-7}
			0.344	2.69×10^{-7}
Laboratory (Neakrase et al., 2006)	1×10^{-3}	4.2×10^{4}	0.060	1.99×10^{-3}
			0.600	1.99×10^{-2}
			0.810	2.69×10^{-2}
			0.470	1.56×10^{-2}
			0.344	1.14×10^{-2}
		9.9×10^{5}	0.060	4.69×10^{-2}
			0.600	4.69×10^{-1}
			0.810	6.34×10^{-1}
			0.470	3.68×10^{-1}
			0.344	2.69×10^{-1}

Figure captions

Figure 1. Topography map based on MOLA data. Dust devil locations detected by HRSC are indicated by the big crosses. Note that one cross does not always represent one orbit/image and mostly not one single dust devil. The crosses stand for the spatial coverage where dust devils have been detected. The numbers in parentheses belong to the above lying crosses except for crosses below the Viking 1 lander region, where the dedicated parentheses are right or left of the crosses. The first number represents the orbit number, the second the number of dust devils seen in this orbit. Highlighted are the landing sites of probes from different missions. The Mars Pathfinder landing site is located at 19°N, 327°E, covered by the Viking 1 writing.

Figure 2. Frequency distribution of 205 dust devils versus season (solar longitude) separated for hemispheres.

Figure 3. Frequency distribution of 205 dust devils versus time of day in one hour bins.

Figure 4. Directions of motion of dust devils plotted on MOLA topography map. White arrows: spring; black arrows: winter; black dashed arrows: fall; related to northern hemisphere. One arrow represents one dust devil direction of motion. If two arrows would overlap each other, only one is plotted. Not for every dust devil in an orbit the direction of motion could be retrieved. a) Dust devils in southern Chryse Planitia/Simud Vallis/Vallis Marineris. b) Dust devils in Peneus Patera.

Figure 5. a) Dust devil in Peneus Patera seen in the ND image (orbit 2133, resolution 25 m/pixel). The black square outlines the location of the SRC image. The scale bar represents

2 km. b) SRC image (resolution 5 m/pixel) revealing many more dust devil tracks than seen in the ND image. Scale bar represents 2 km. c) An enlargement of the dust devil seen in the SRC image, showing the kink between the lower and the upper part of the dust devil. Scale bar represents 400 m. North is to the top of each image.

Figure 6. ND image of Noachis Terra (orbit 2225) showing four dust devils (outlined by white circles) and their tracks. North is to the top of the image. The scale bar represents 2 km.

Figure 7. HRSC ND images showing some of the best image dust devils; north is to the top. a) Five dust devils in Thaumasia Planum (orbit 1081) in one row. Scale bar represents 8 km. b) Five dust devils in Syria Planum (orbit 2054) located in front of a dust storm. Scale bar represents 3 km.

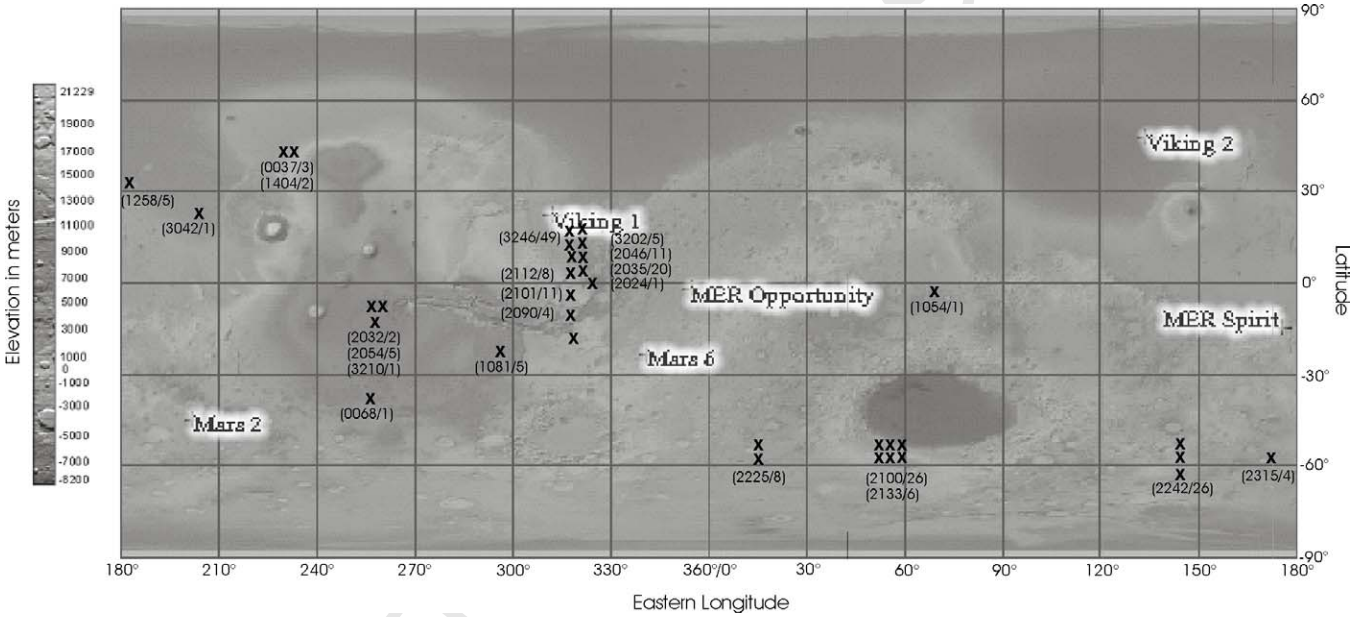

I10159_Fig1

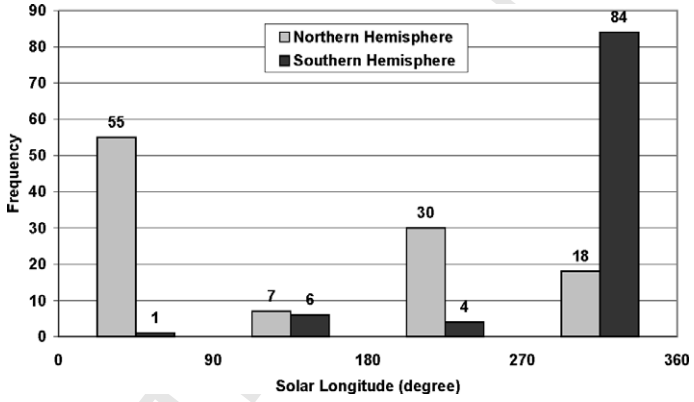

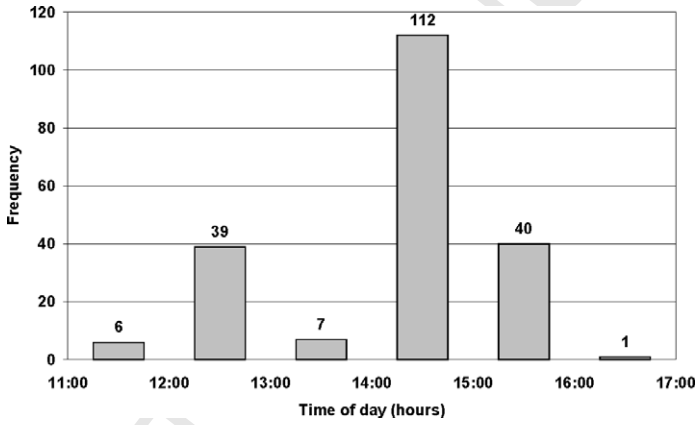

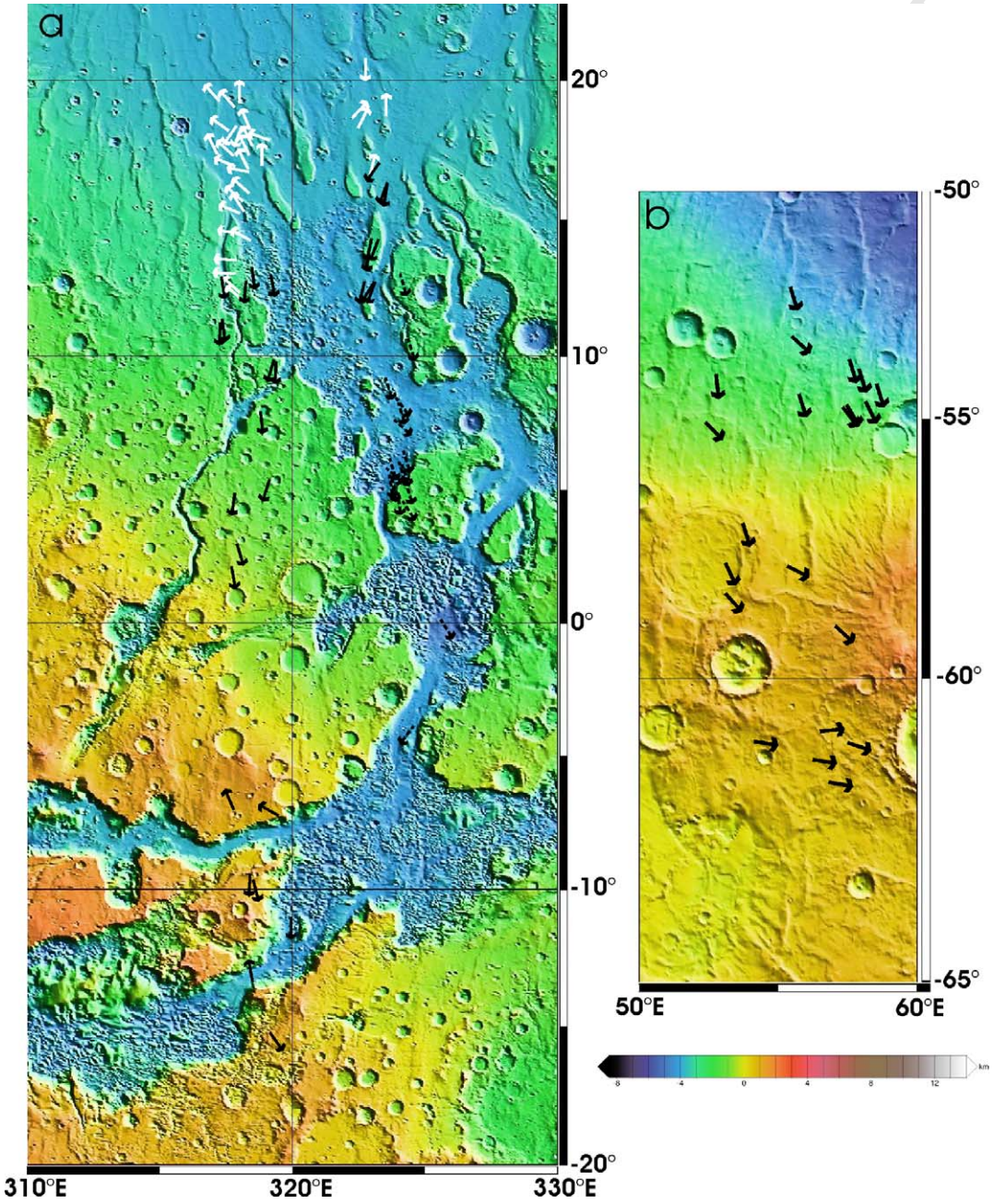

I10159_Fig4

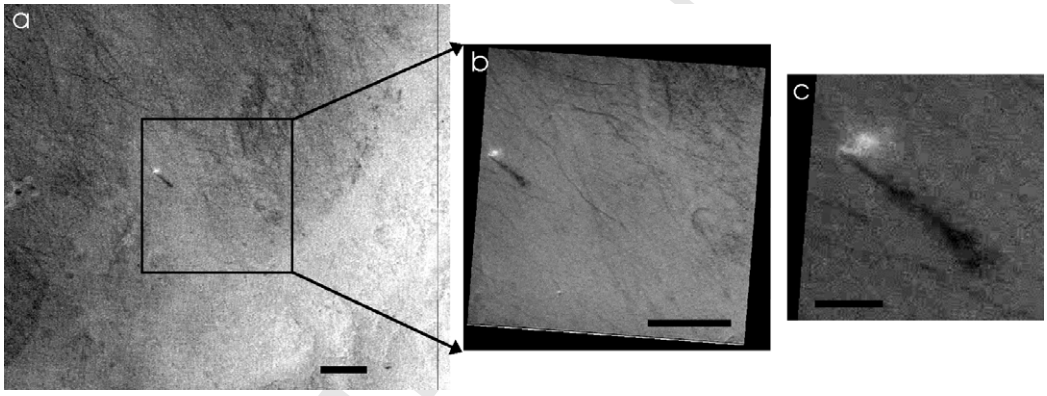

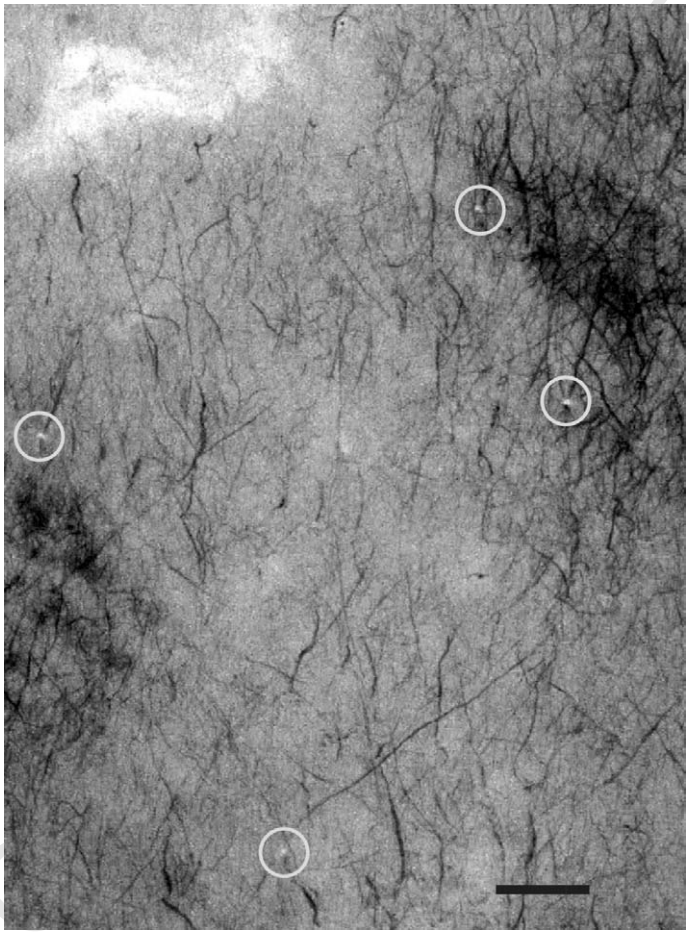

I10159_Fig6